Network-Motif Delay Differential Analysis of Brain Activity During Seizures

Claudia Lainscsek[*,1,3], Pariya Salami[*,4], Vinícius Rezende Carvalho[*,6,7,8], Eduardo M. A. M. Mendes[8], Miaolin Fan[4], Sydney S. Cash[4], and Terrence J. Sejnowski[1,3,5]

[*] *These authors contributed equally to this work.*

[1] *Computational Neurobiology Laboratory, The Salk Institute for Biological Studies, 10010 North Torrey Pines Road, La Jolla, CA 92037, USA*

[2] *Department of Neurosciences, University of California San Diego, La Jolla, CA 92093, USA*

[3] *Institute for Neural Computation, University of California San Diego, La Jolla, CA 92093, USA*

[4] *Department of Neurology, Massachusetts General Hospital and Harvard Medical School, Boston, MA 02114, USA*

[5] *Division of Biological Sciences, University of California San Diego, La Jolla, CA 92093, USA*

[6] *Department of Psychology, University of Oslo, Forskningsveien 3A, 0373 Oslo, Norway*

[7] *RITMO Centre for Interdisciplinary Studies in Rhythm, Time and Motion, University of Oslo, Forskningsveien 3A, 0373 Oslo, Norway*

[8] *Laboratório de Modelagem, Análise e Controle de Sistemas Não Lineares, Universidade Federal de Minas Gerais, Av. Antônio Carlos 6627, 31270-901 Belo Horizonte, MG, Brazil*

(Dated: October 11, 2023)

Delay Differential Analysis (DDA) is a nonlinear method for analyzing time series based on principles from nonlinear dynamical systems. DDA is extended here to incorporate network aspects to improve the dynamical characterization of complex systems. To demonstrate its effectiveness, DDA with network capabilities was first applied to the well-known Rössler system under different parameter regimes and noise conditions. Network-Motif DDA (NM-DDA), based on cortical regions, was then applied to invasive intracranial electroencephalographic (iEEG) data from drug-resistant epilepsy patients undergoing presurgical monitoring. The directional network motifs between brain areas that emerge from this analysis change dramatically before, during, and after seizures. Neural systems provide a rich source of complex data, arising from varying internal states generated by network interactions.

Epilepsy is a neural network disorder that affects over fifty million people worldwide. Although some patients benefit from current medical treatments, many still have seizures that are refractory. Despite advances made in the diagnosis and treatment of epilepsy, the proportion of patients who are free of seizures following treatment has not changed. Epilepsy manifests in a wide range of symptoms and conditions, with influence that often extends far beyond the regions of seizure onset. Recent methods aimed at uncovering the network dynamics of brain activity allow seizures to be investigated in ever greater detail. Here we use NM-DDA, a new flavor of delay-differential analysis, to explore and better understand how seizures originate, the pathways through which they propagate, and how they eventually terminate.

I. INTRODUCTION

Complex systems often display emergent properties and are challenging to investigate. When the whole is greater than the sum of its parts, reductionist descriptions are not enough to understand, predict or control its behavior. Examples of such systems are abundant in physics, climate studies, economics, and biology [44, 49]. Thus, developing frameworks to investigate complex networks and uncover common principles between seemingly very different systems or domains is an active and promising research direction. Critical elements of such a framework include nonlinear dynamics, statistical physics, and network theory [1].

The activity of the brain is a preeminent example of such a complex system and is challenging for the study of networks. Complex network dynamics underlie cognition and consciousness [46], and disruptions of these networks on different spatiotemporal scales lead to neurological conditions that are characterized by abnormal synchronization and coupling between neuronal populations [47]. The most common examples of these include Alzheimer's disease [43], schizophrenia [26], autism spectrum disorder [9], Parkinson's disease [10], and epilepsy [36]. Among these conditions, epilepsy is a network disorder [13, 52] with special interest for network theory due to its inherently dynamical nature. Abnormal synchronization and network dynamics are increasingly recurring themes in the theories and models of epilepsy [3], and may be responsible for the pharmacological resistance in 20-30% of cases, which has not dropped in decades despite the development of new treatments [5].

Changes in the functional or effective connectivity are involved in the initiation [38, 50], spreading [12], and termination of seizures [13, 48]. These changes may support clinical decisions in cases of intractable focal epilepsy by providing a better assessment of the putative epileptogenic zones that are candidates for surgical resection [24].

Epileptogenic or seizure onset zones [42, 52] are at the tip of epileptogenic networks involving interactions with other critical nodes that generate and maintain seizures. This has implications for the forecasting [4, 8, 31], control, and suppression of seizures [11, 29], in addition to other targeted (mainly surgical) interventions [2, 24]. In all of these cases, neural activity is supported by network dynamics [30] and interactions occur between neural populations at different spatiotemporal scales [15, 51]. Understanding the relevant neural dynamics, which are often nonlinear, is key to providing useful insights into ameliorating seizure treatment.

Delay differential analysis (DDA) [16–18, 21] is a classification tool that has been used extensively for analyzing neural data, including iEEG recordings during epileptic seizures. It has several variations that capture different aspects of interacting dynamics in nonlinear systems. However, what has been lacking so far is a focus on the network aspects underlying dynamics. In this paper, we aim to integrate DDA with network constraints to better characterize complex systems. We analyzed data from two nonlinear systems: (i) the well-known model Rössler system with different parameters and noise conditions, and (ii) invasive intracranial electroencephalographic (iEEG) recordings from epilepsy patients undergoing presurgical monitoring.

The paper is organized as follows: Section II describes DDA and its different flavors or versions; Section III introduces the proposed addition to the DDA framework and demonstrates its use in simulated data from coupled Rössler systems; Section IV contains results of the proposed approach with real invasive iEEG data from two epilepsy patients before, during, and after seizures. Discussion of results and conclusions are given in Section V.

II. THE FLAVORS OF DDA

DDA is a detection/classification framework that combines differential embeddings with linear and nonlinear nonuniform functional delay embeddings [32, 40, 45] to relate the current derivatives of a system to the current and past values of the system variables [14, 17, 23].

More traditional analyses that are often based on spectral features have hundreds of features per data segment and approaches based on artificial neural networks increase even further the feature space. Therefore, such techniques rely on dimensionality reduction techniques to achieve a viable number of features. DDA, on the other hand, achieves a reduced feature space by mapping the data on a "natural" nonlinear basis (inspired by Max Planck's "natural units" [34]) that is selected according to the classification problem. Therefore, DDA is efficient at embedding the meaningful dynamics of the data in a low-dimensional DDA model of only three terms. This has several advantages: it is noise-insensitive, less prone to overfitting, and computationally fast and therefore making it a useful tool for analyzing real world iEEG data [6, 16–19, 22, 39].

DDA has four flavors:

1. Single-Trial/Channel DDA (ST-DDA) [22] is the classical variant developed for analyzing single time series.
2. Cross-Trial/Channel DDA (CT-DDA) [20] determines the overall dynamics of multiple time series simultaneously.
3. Dynamical-Ergodicity DDA (DE-DDA) [16] is a combination of ST-DDA and CT-DDA to assess dynamical ergodicity or similarity from data.
4. Cross-Dynamical DDA (CD-DDA) [17] measures causality between two time series.

We introduce here Network-Motif DDA (NM-DDA) for network analysis, which uses a combination of all four DDA flavors above. In the next section, we introduce this analysis framework on simulated data of coupled Rössler systems; but first, we want to remind the reader of the four flavors of DDA in detail.

A. ST-DDA

Single Trial/Channel DDA is used for analyzing a single time series. To do that we first have to select the DDA model that best fits the overall dynamics of the data.

The general nonlinear DDA model with two time delays and three terms is

$$\begin{aligned} \dot{u}(t) &= \sum_{i=1}^{3} a_i \, u(t-\tau_1)^{m_i} \, u(t-\tau_2)^{n_i} \\ \dot{u} &= \mathcal{F}_u + \rho_u \end{aligned} \tag{1}$$

where $u(t)$ is a time series and ρ_u is the fitting error and noise term. The nonlinearity is specified by $m_i, n_i, \tau_{1,2} \in \mathbb{N}_0$ and a degree $m_j + n_j \leq 4$. The noise and residuals are obtained through data analysis: First the upper line in Eq. (1) with $m_1 + n_1 \geq 1$ is solved by excluding a constant term to estimate the three coefficients $a_{1,2,3}$ using singular value decomposition (SVD) [35]. Then the noise term ρ_u in the second line in Eq. (1) is estimated as the least square fitting error $\rho_u = \sqrt{\sum(\dot{u} - \mathcal{F}_u)^2}$. For stationary data and a DDA model with an infinite number of parameters, e.g. a Volterra series, the constant term would be the noise term. For a sparse model of only three terms, as used in DDA, the constant term includes the noise as well as the fitting error of the model. The derivative on the left side is computed using a center derivative algorithm [27, 28].

The model form of Eq. (1) has to be chosen to fit the overall nonlinear orchestration of the data. For the two data sets in this paper, the simulated data from coupled

Rössler systems and real iEEG data from epilepsy patients, the models were chosen by minimizing the error ρ. For the simulated uncoupled Rössler data we did an exhaustive search over all three term models with two delays up to a cubic order of nonlinearity and all delays between 6 and 60 δt, where δt is the time step for numerical integration. For the iEEG data from epilepsy patients we used a genetic algorithm as explained in [22] to find the best model form and delays simultaneously. Data (recorded with a 500 Hz sampling rate) from 13 patients were used for this search. They consisted of a million randomly selected two second data segments around the 155 seizures (half an hour before to half an hour after seizure onset as marked by neurologists) from 730 iEEG channels. Interestingly, most of the models chosen consisted of two linear and one nonlinear term. Two of those models had a mean high error before and a low error after seizure onset. These models are

$$\begin{aligned} \dot{u} &= a_1\, u_1 + a_2\, u_2 + a_3\, u_1^2 \\ \dot{u} &= a_1\, u_1 + a_2\, u_2 + a_3\, u_1^4 \end{aligned} \tag{2}$$

where we abbreviated $u(t-\tau_\star) = u_\star$ to have a more compact notation and be consistent with previous publications. We use here the second model because we want to use only one and it proved slightly better in the past. The genetic algorithm selected 8 delay pairs and all of those were used in [22]. We chose here one of the delay pairs that proved to be useful for the analysis of epilepsy iEEG data. Here, the delays $\tau_1 = 7\ \delta t, \tau_2 = 10\ \delta t$ are employed, where δt is the sampling time corresponding to a sampling rate of $f_s = 500$Hz.

To better explain how ST-DDA extends to the other DDA flavors we apply the DDA iEEG model to a time series $u(t)$ of length L and rewrite it as matrix equation in the following way:

$$\dot{u} = a_1\, u_1 + a_2\, u_2 + a_3\, u_1^4$$

$$\begin{pmatrix} \dot{u}(t+1) \\ \dot{u}(t+2) \\ \dot{u}(t+3) \\ \vdots \\ \dot{u}(t+L) \end{pmatrix} = \begin{pmatrix} u(t+1-\tau_1) & u(t+1-\tau_2) & u(t+1-\tau_1)^4 \\ u(t+2-\tau_1) & u(t+2-\tau_2) & u(t+2-\tau_1)^4 \\ u(t+3-\tau_1) & u(t+3-\tau_2) & u(t+3-\tau_1)^4 \\ & \vdots & \\ u(t+L-\tau_1) & u(t+L-\tau_2) & u(t+L-\tau_1)^4 \end{pmatrix} \begin{pmatrix} a_1 \\ a_2 \\ a_3 \end{pmatrix} \tag{3}$$

$$\dot{\mathbf{u}} = \mathbf{M_u}\, \mathbf{A}$$

Note, that $\mathbf{M_u}$ is an $(L \times 3)$ matrix. L is the number of data points for each window for the estimation of the three free parameters $a_{1,2,3}$. It needs to be of sufficient length to capture the embedded dynamics of the time series while remaining concise enough to detect changes in those dynamics, making it inherently dependent on the data. Its choice also depends on the timescale of the dynamics of interest. For the Rössler data we use 2000 data points for a integration step size of $\delta t = 0.025$ and for the epilepsy data we use a quarter of a second, which gives 125 data points for a sampling rate of 500 Hz.

B. CT-DDA

Multiple time series can be analyzed with CT-DDA. For two time series, $u_1(t)$ and $u_2(t)$, the features can be either computed for each time series separately, resulting in $(\mathbf{A}, \rho_a)_1$ and $(\mathbf{A}, \rho_a)_2$, or in a combined way by solving the equation

$$\begin{pmatrix} \dot{\mathbf{u}}_1 \\ \dot{\mathbf{u}}_2 \end{pmatrix} = \begin{pmatrix} \mathbf{M_{u}}1 \\ \mathbf{M_{u}}2 \end{pmatrix} \mathbf{B} \tag{4}$$

for the features $\mathbf{B} = (b_1, b_2, b_3)$. In (4), the vector $\begin{pmatrix} \dot{\mathbf{u}}_1 \\ \dot{\mathbf{u}}_2 \end{pmatrix}$ has $2L$ elements since the two time series $u_1(t)$ and $u_2(t)$ are each of length L. $\begin{pmatrix} \mathbf{M_{u}}1 \\ \mathbf{M_{u}}2 \end{pmatrix}$ is a $(2L \times 3)$ matrix and $\mathbf{M_{u}}1$ and $\mathbf{M_{u}}2$ each have the same form as $\mathbf{M_u}$ in Eq. (3). Therefore, $\mathbf{B} = (b_1, b_2, b_3)$ is a vector with three elements. This can be extended to any number of time series. Note that for ST-DDA, there are as many feature sets $(\mathbf{A}, \rho_a)$ as there are time series, while for CT-DDA there is only one combined feature vector $(\mathbf{B}, \rho_b)$.

CT-DDA only makes sense if the dynamics in the two time series $u_1(t)$ and $u_2(t)$ are similar and therefore can be used to test for dynamical similarity. This motivates dynamical ergodicity.

C. DE-DDA

Consider two time series $u_1(t)$ and $u_2(t)$ and the two corresponding ST-DDA feature vectors $(\mathbf{A}, \rho_a)_1$ and $(\mathbf{A}, \rho_a)_2$. From CT-DDA there is one combined feature vector $(\mathbf{B}, \rho_b)$. The mean of the two ST-DDA errors, $\overline{\rho_a}$, and the CT-DDA error ρ_b should be similar if the analyzed time series have similar dynamics and the quotient should be close to one. *Dynamical Ergodicity* as used in DE-DDA is defined as:

$$\mathcal{E} = \left| \frac{\overline{\rho_a}}{\rho_b} - 1 \right| . \tag{5}$$

D. CD-DDA

For CD-DDA we consider two dynamical systems X and Y resulting in the time series $u(t)$ and $v(t)$. the first step is to compute a set of features $\mathbf{C} = (c_1, c_2, c_3)$ with

$$\dot{\mathbf{u}} = \mathbf{M_u}\, \mathbf{C} + \rho_u \tag{6}$$

where $\dot{\mathbf{u}}$ is a vector of length L and the delay matrix $\mathbf{M_u}$ is a $(L \times 3)$ matrix. To check if there is a causal connection from Y to X, we add the delay matrix from the other time series, $\mathbf{M_v}$, to the equation

$$\dot{\mathbf{u}} = (\mathbf{M_u}\, \mathbf{M_v})\, \mathbf{E} + \rho_{uv} . \tag{7}$$

$(\mathbf{M_u}\,\mathbf{M_v})$ now is a $(L \times 6)$ matrix resulting in $\mathbf{E} = (e_1, e_2, \ldots, e_6)$ with six elements. If there is a causal connection from Y to X, then the last three elements of $\mathbf{E}$ will make the model better and the error ρ_{uv} should decrease. If there is no causal connection from Y to X, then the last three elements of $\mathbf{E}$ will be irrelevant and the error ρ_{uv} should not change. The difference

$$\mathcal{C}_{uv} =\mid \rho_u - \rho_{uv} \mid \tag{8}$$

can therefore be used to quantify causality from Y to X. A causal connection from X to Y can be tested in the same way, starting with

$$\dot{\mathbf{v}} = \mathbf{M_v}\,\mathbf{D} + \rho_v \tag{9}$$

where $\dot{\mathbf{v}}$ is a vector of length L and $\mathbf{M_v}$ is a $(L \times 3)$ matrix. Once again, the second delayed matrix $\mathbf{M_u}$ can be added to the equation,

$$\dot{\mathbf{v}} = (\mathbf{M_u}\,\mathbf{M_v})\,\mathbf{F} + \rho_{vu}\,. \tag{10}$$

$(\mathbf{M_u}\,\mathbf{M_v})$ is the same combined $(L \times 6)$ delay matrix as in Eq. (7) resulting in $\mathbf{F}$ with six elements. Whether the first three terms of $\mathbf{F}$ are relevant or not tells us whether there is a causal connection and

$$\mathcal{C}_{vu} =\mid \rho_v - \rho_{vu} \mid \tag{11}$$

is used to quantify causality from X to Y.

However, this and all other causality measures assume that the two dynamical systems are not entirely similar or synchronized to each other. Adding Dynamical Ergodicity and looking at $\mathcal{E} * \mathcal{C}$ adjacency matrices eliminates spurious incorrect connections that result from non-independent systems.

III. NETWORK ANALYSIS ON SIMULATED DATA OF THE RÖSSLER SYSTEM

To first test the framework, we use simulated data of the Rössler system [37]. This system is a three-dimensional system of ODEs with one nonlinearity that was introduced by Rössler as a simplification of the Lorenz system [25]. One reason it serves as a benchmark system is that, despite its relative simplicity, it can generate a wide variety of dynamical behaviors, including chaos. We couple Rössler systems using diffusive coupling as introduced in Paluš and Vejmelka [33] and consider here seven (coupled) Rössler systems

$$\begin{aligned} \dot{x}_n &= -y_n - z_n + \sum_j \epsilon(x_n - x_j) \\ \dot{y}_n &= x_n + a_n\, y_n \\ \dot{z}_n &= b_n + c_n z_n + x_n z_n \end{aligned} \tag{12}$$

with $n = 1, 2, \ldots, 7$ and x_j is the x-component of another system. The values for a_n, b_n, and c_n are listed in Tab. I. ϵ is either 0 or 0.15 depending on which systems are coupled. The seven Rössler systems were integrated with a step size of 0.05 and down-sampled by a factor of two. We ran this experiment in three segments: (i) seven uncoupled systems, (ii) systems #(4,5,6)→#7 with $\epsilon = 0.15$, and (iii) #7→#(4,5,6) with $\epsilon = 0.15$ (see Fig. 1). This experiment was first run without noise and then repeated for added white noise with a signal to noise ratio (SNR) of 15 dB. Fig. 1 shows the embeddings of one data window of 2000 data points for each of the seven x_n time series from Eq. (12) for no noise and added white noise of SNR=15 dB. For the remainder of this section the three different cases will have the same backgrounds in the figures.

TABLE I: Parameters of the seven Rössler systems

#	a_n	b_n	c_n
1	0.21	0.21505	4.5
2	0.21	0.20201	4.5
3	0.21	0.20411	4.5
4	0.20	0.40503	4.5
5	0.20	0.39905	4.5
6	0.20	0.41000	4.5
7	0.18	0.50000	6.8

For the DDA part we chose a window length of 2000 data points and a window shift of 500 data points. We used the same model and delays as in [17]:

$$\dot{u} \;=\; a_1\, u_1 + a_2\, u_2 + a_3\, u_1^3 \tag{13}$$

with $u_j = u(t - \tau_j)$, $\tau_1 = 32\ \delta t$, $\tau_2 = 9\ \delta t$, and $\delta t = 0.025$. We computed DE-DDA ($\mathcal{E}$) as explained in [16] for all pairwise combinations of the seven x_n components of the seven Rössler systems in Eq. (12). The lower the value of $\mathcal{E}$ the more dynamically similar the data are. The middle panel in Fig. 2 shows them as function of time for a few data windows. The bottom plots show the resulting dynamical ergodicity matrices for three time windows. These three time windows were chosen before the network switch on, for a data window with data from before and after switch on, and a data window after network switch on. The corresponding networks are shown in the top panel. Fig. 3 shows the same for the whole time series and 500 data windows for each case. Lighter colors represent a lower $\mathcal{E}$ value and higher dynamical similarity. As can be seen in Fig. 3 for the unconnected case systems #(1,2,3), #(4,5,6), and #7 are clearly similar. For case (ii), where #(4,5,6)→#7 system #7 is clearly different, while all other systems are similar to each other, forming 2 groups, namely #(1,2,3) and #(4,5,6). For case (iii), where #7→#(4,5,6) systems #(1,2,3) are most different to all other systems and #(4,5,6) can still be distinguished from #7.

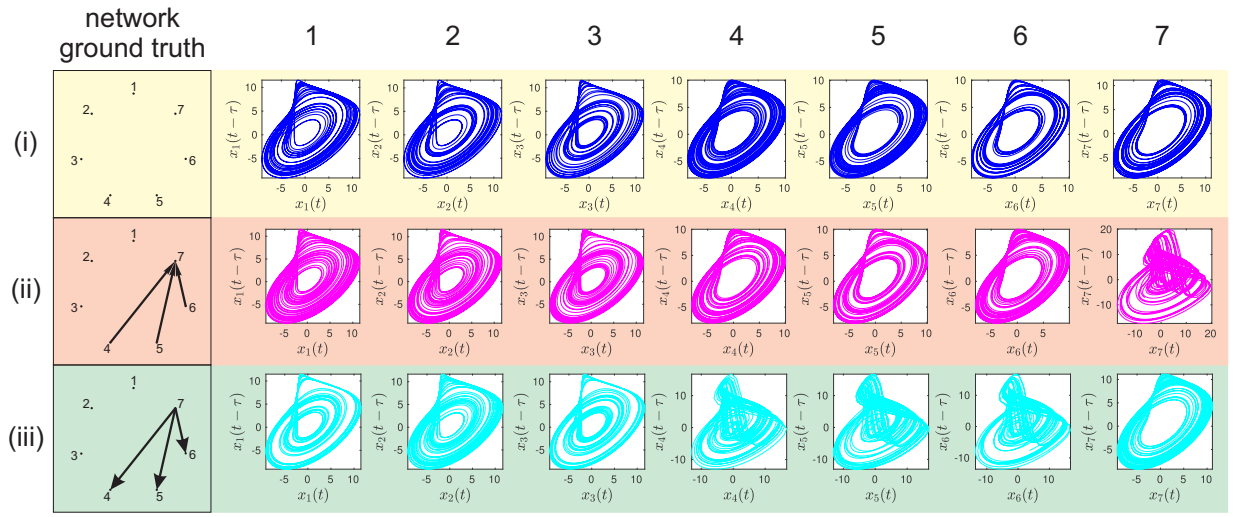

(a)No noise

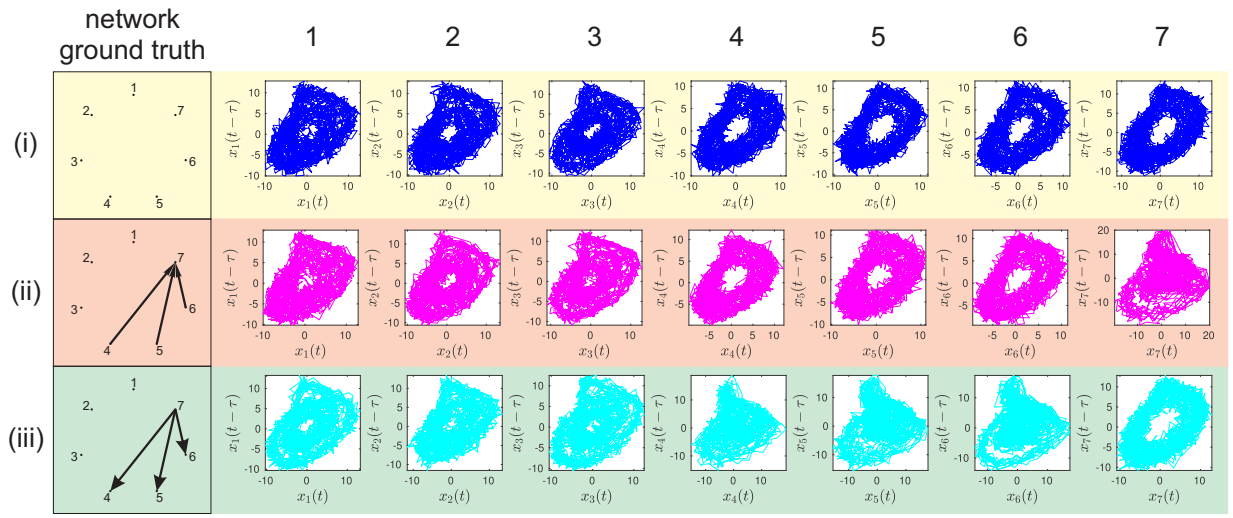

(b)Added white noise with SNR=15 dB

FIG. 1: **Comparisons of the embeddings of the seven Rössler systems in Eq. (12) with (a) No noise added and with (b) Added white noise.** For each graph one data window (2000 data points) with $\tau = 10\delta t$ of the x_n components is shown. The rows correspond to the three cases, (i) seven uncoupled systems, (ii) systems #(4,5,6)→#7 with $\epsilon = 0.15$, and (iii) #7→#(4,5,6) with $\epsilon = 0.15$. In the boxes on the left the network motifs for these three cases are shown. The numbers in the network motifs correspond to the seven systems.

To recover the network structure we first computed the causality measure $\mathcal{C}$ using CD-DDA. The results are shown in Fig. 4. The upper panel shows causality from the seven systems to all other systems as function of time. Each vertical line represents an adjacency matrix. The mean of all adjacency matrices for each of the three cases is shown in the middle panels. These can also be plotted as network graphs in the bottom panel. To display the network graphs we disregard the lower 25% of the values in the adjacency matrices. For case (i) we get incorrect connections between the groups of systems that are similar. For the cases (ii) and (iii) the right connections are bigger than additional incorrect connections. All incorrect connections result from dynamical similarity. In such cases causality is not meaningful. As explained in [16] we therefore multiply $\mathcal{C}$ with $\mathcal{E}$ and show the results in Fig. 5. Now, all the incorrect connections disappeared and we recovered the correct networks for all three cases. For the unconnected network in case (i) all values are very small and much smaller than for the other two cases.

In the next step we did principal component analysis (PCA) [35] and computed the first principal component and first singular value from 100 $\mathcal{E} * \mathcal{C}$ adjacency matrices with sliding windows over time. This analysis makes more sense for real data where we have changes of network connections over time that might e.g. lead to epileptic seizures. From Fig. 6 we can see, that the first singular value in case (i), the unconnected systems, is close to zero, while it is bigger for connected systems. Other SVs

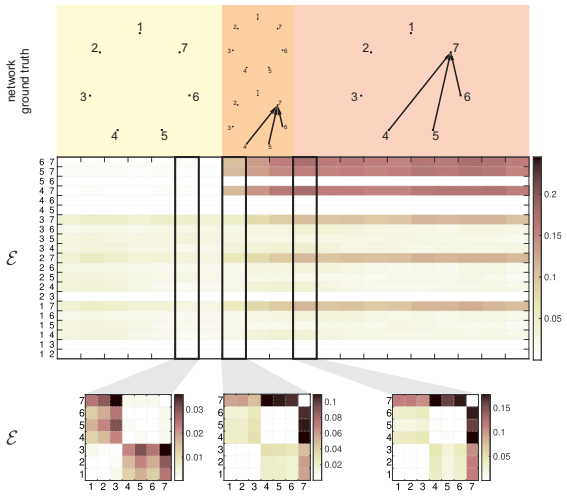

FIG. 2: **Transitional DDA time windows.** The top panels show the network motifs on the left and right. In between there is a transitional time of 2000 data points (window length) where the analysis shifts from the left to the right motif. In the middle panel the temporal evolution of the stratified dynamical ergodicity matrices is shown. The lower panel shows the mean of three ergodicity matrices over 2000 data points before, during, and after the transition. After and during the transition the three different types of dynamics are more obvious indicated by much higher values of $\mathcal{E}$ than for the uncoupled network. Lower values of the dynamical ergodicity $\mathcal{E}$ correspond to higher dynamical similarity.

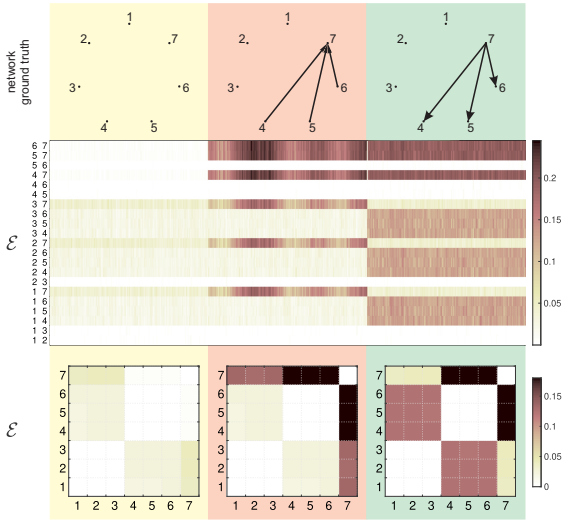

FIG. 3: **Transitional DDA time windows for the whole time series.** Network motifs (top panel), dynamical ergodicity as function over time (middle panel), and dynamical ergodicity matrices (bottom panel) for the 7 time series of the x-components of the Rössler systems. This figure shows the same properties as Fig. 2 on a bigger time scale.

could also be used for characterizing the dynamics, but for the sake of simplicity and demonstrating the method, we only used one. For the simple dynamics of the simulated Rössler data adding additional SVs was not necessary to improve the method. In the case of the epilepsy data we need to look at more patients, which is planned for a more medical oriented audience, to investigate the importance of the other SVs.

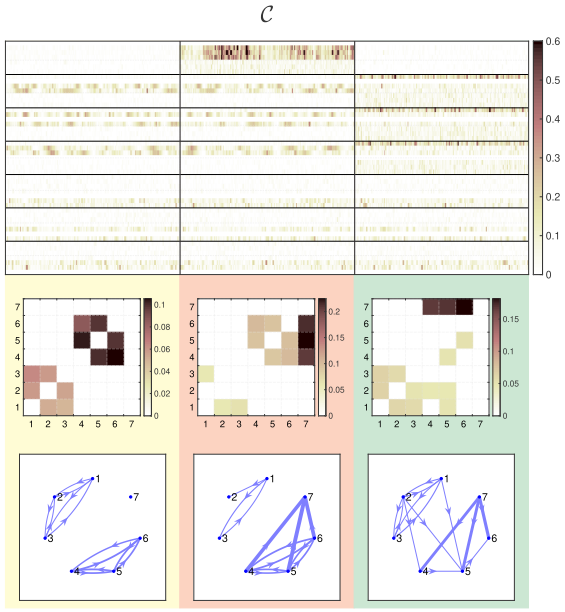

FIG. 4: **Causality $\mathcal{C}$ for three different networks.** The top panel shows the stratified adjacency matrices $\mathcal{C}$ for the three cases, (i) seven unconnected systems (12), (ii) #(4,5,6)→#7, and (iii) #7→#(4,5,6). The middle panel shows the mean adjacency matrices for each case and the bottom panel shows the resulting network motifs where the lower quarter of values was disregarded. The line widths indicate the connection strengths. This figure clearly points out that $\mathcal{C}$ alone causes spurious connections and needs improvement.

To check how the analysis reacts to noise we added white noise of SNR=15 dB to the data and repeated all previous steps. Fig. 7 shows the reconstructed networks. Again, the connections in cases (ii) and (iii) were identified correctly. For case (i) the values of the connections are very small and the first singular value is close to zero.

To summarize our findings on simulated data, causality $\mathcal{C}$ alone often shows incorrect connections because the systems are very similar (see also [17] for more examples and comparison to other methods such as Granger causality, transfer entropy, and convergent cross mapping). Adding Dynamical Ergodicity and looking at $\mathcal{E} * \mathcal{C}$ adjacency matrices eliminates those incorrect connections but for unconnected systems weak connections between the nodes of similar dynamics appear. Adding PCA analysis eliminates those.

We will apply this framework in the next section to iEEG data from epilepsy patients to identify network motifs related to epileptic seizures.

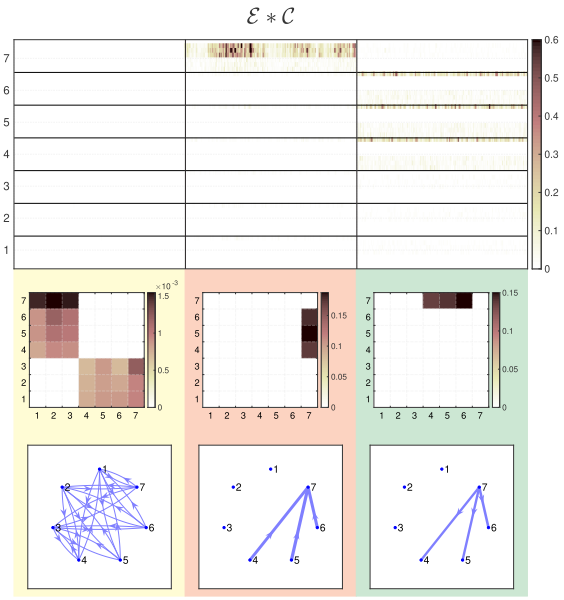

FIG. 5: $\mathcal{E} * \mathcal{C}$ **for three different networks.** The top panel shows the stratified adjacency matrices $\mathcal{E} \star \mathcal{C}$ for the three cases. The middle panel shows the mean adjacency matrices for each case and the bottom panel shows the resulting network motifs where the lower quarter of values was disregarded. The line widths indicate the connection strengths. This figure is a clear improvement over Fig. 4 for the coupled systems. In those two cases on the right only correct connections are captured. The very left part for the unconnected network still shows spurious connections but with much lower values. Further improvement is needed.

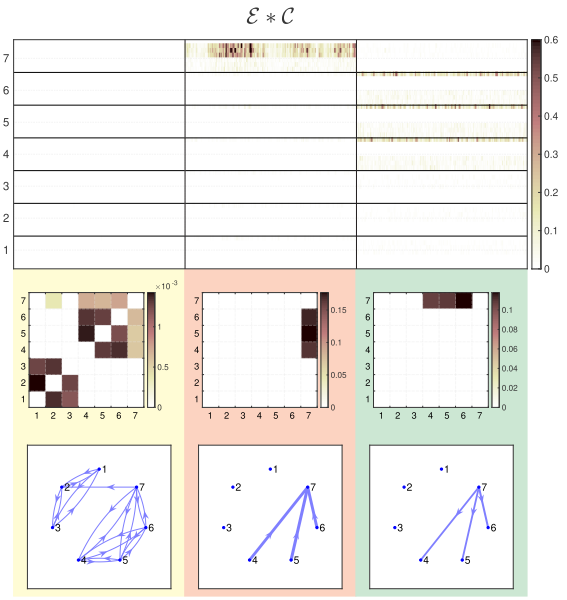

FIG. 7: $\mathcal{E} * \mathcal{C}$ **for three different networks with noise.** The top panel shows the stratified adjacency matrices $\mathcal{E} \star \mathcal{C}$ for the three cases. The middle panel shows the mean adjacency matrices for each case and the bottom panel shows the resulting network motifs where the lower quarter of values was disregarded. The line widths indicate the connection strengths. White noise of 15 dB was added to the data. This figure should be compared to Fig. 5 where the noise-free case is shown.

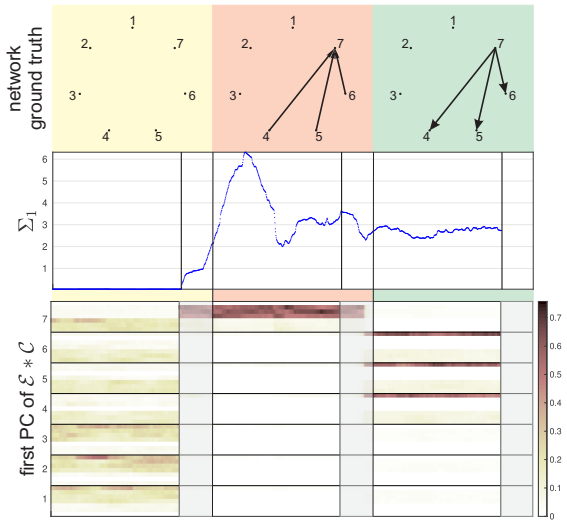

FIG. 6: **First singular value Σ (middle panel) and first principal component (bottom panel) of the $\mathcal{E} * \mathcal{C}$ adjacency matrices in Fig. 5.** The grey boxes indicate transitional windows between the cases. The top panel shows the ground truth network motifs. This figure is a clear improvement over Fig. 5 where spurious connections have small singular values.

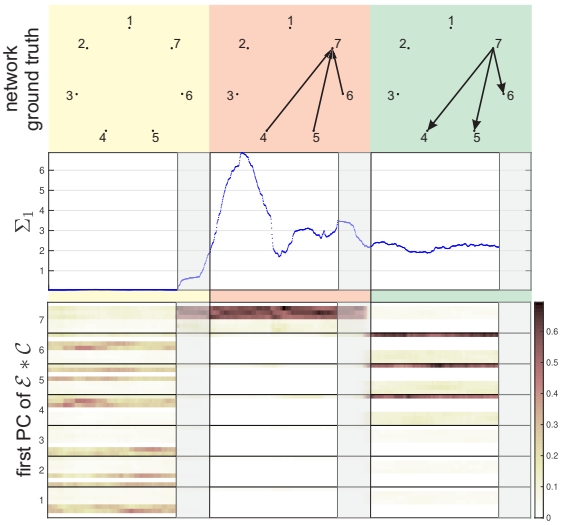

FIG. 8: **First singular value Σ_1 (middle panel) and first principal component (bottom panel) of the $\mathcal{E} * \mathcal{C}$ adjacency matrices in Fig. 7.** White noise of 15 dB was added to the data. The grey boxes indicate transitional windows between the cases. The top panel shows the ground truth network motifs. This figure should be compared to Fig. 6 where the noise-free case is shown.

IV. EPILEPSY DATA

In [22] a genetic algorithm was used to select the model with minimum error from one second data segments for one hour periods centered on the seizure onset times. Around one million such data segments (155 seizures and 730 iEEG channels from 13 patients) were analyzed in this way. The patient demographics and characteristics are described in [22]. All data were obtained with informed patient consent and handled following protocols as approved by the IRB of the Massachusetts General Hospital.

The DDA model selected in [22] for the characterization of epileptic seizures is

$$\dot{u} = a_1 u_1 + a_2 u_2 + a_3 u_1^4 \tag{14}$$

with $u_i = u(t - \tau_i)$. We use overlapping data windows of 250 ms length with a window shift of 25 ms. We did not filter or pre-process the data except normalizing each data window to zero mean and unit variance. Here, we show results from two patients.

Since the patients in our data set have from around 80 to over 300 electrodes implanted, the networks may be complex and heterogeneous. We therefore compute the DDA features $a_{1,2,3}$ and the error ρ for each channel as well as $\mathcal{E}$ and $\mathcal{C}$ for each pairwise channel combination. We then group channels according to brain region or network and take the mean of the DDA features. Mapping of channels to brain areas was done with an electrode labeling algorithm (ELA) [7, 41], and grouped into eight major regions indicated by

Brain Region	Abbreviation
frontoparietal	FP
cingulate	CG
lateral temporal	AT
mesial temporal	MT
hippocampus	HP
occipital	OC
thalamus	TH
subcortical	SU

and are preceded by R or L to indicate the right or left hemisphere. We then use the same template for all network motifs. An example is shown in Fig. 9. Brain regions without implanted electrodes are indicated with a dot. The line widths indicate the connection strength. The lower quarter of values in the $\mathcal{E} * \mathcal{C}$ adjacency matrices were disregarded.

In Fig. 10 the value of a_1 is shown as function over time from 2 minutes before seizure onset to 2.5 minutes after as determined by the neurologist. In [22] we showed a similar plot according to the channels. Here we sorted the channels according to the brain regions we used for the network analysis.

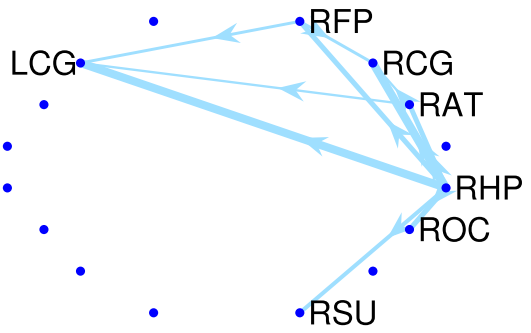

FIG. 9: **Example of a network motif.** Thickness of the lines indicates strength of coupling between brain regions. Each hemisphere was divided into eight cortical and subcortical areas indicated by dots. Since in most cases not all of the 16 regions are covered by implanted electrodes dots without labels represent regions without electrodes.

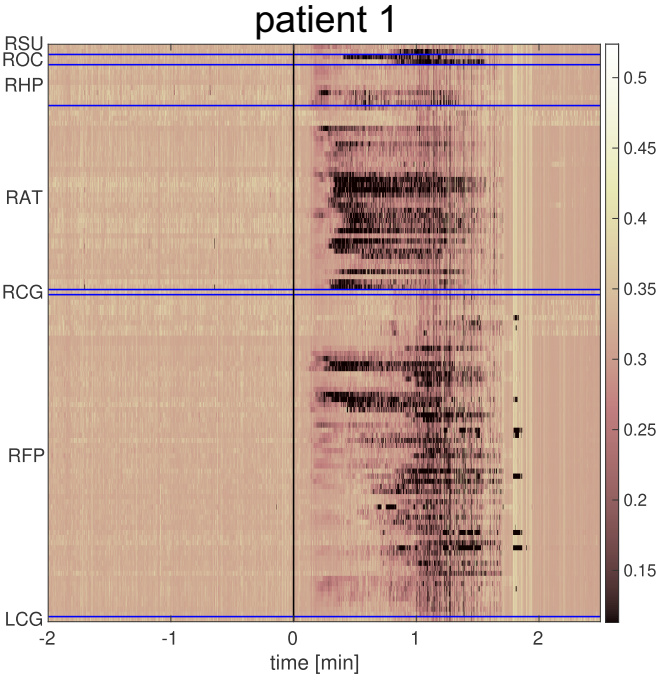

FIG. 10: **Coefficient a_1 of seizure #4 of patient 1 from 2 minutes before seizure onset to 2.5 minutes after.** The channels were sorted according to the brain regions used for network analysis. A similar plot without sorting was shown in [22]. This plot indicates where the seizure starts and how it progresses across different channels and regions.

In Fig. 11 the $\mathcal{E} * \mathcal{C}$ causality is shown as function of time along with the first principal component. The gray box before seizure onset at time 0 indicates the window used for PCA.

In Fig. 12 the first singular value is shown from 2 minutes before to 2.5 minutes after seizure onset, as determined by the neurologist. The network motifs are plotted every 20 seconds from 20 seconds before to 100 seconds after

seizure onset. We then correlated the first PCs of those time points with the first PCs across time to see if some motifs are distinct seizure-related motifs. In Fig. 13 these correlations are shown in the upper plot in the same colors as the lines and network motifs in Fig. 12. In the lower plot of Fig. 13 the values of these lines are shown as colors. There are clearly distinct network motifs before, during, and after the seizure. We then computed the first singular values and the correlations to the same network motifs from 10 minutes before seizure #4 (the same as in the previous plots) to 10 minutes after seizure #5. This plot shows clear evidence that there are distinct network motifs related to the epileptic seizures of this patient. We see the same behavior for all seizures of this patient.

Comparing the correlations of the first PCs to data between two seizures (we chose the seizures closest together in time for the two patients) we can see some similarities: For patient 1 in Fig. 14 around 3 hours of data are shown. The singular values have big peaks for the 2 seizures and there are distinct correlations of the first PCs to the rest of the data indicating distinct network motifs related to the different phases of the seizures that do not occur in between the seizures. For patient 2 in Fig. 15 around 2 hours of data are shown. The singular values have peaks for the two seizures but show also activity in between. The correlations of the first PCs to the rest of the data are again distinct network motifs related to the different phases of the seizures that do not occur in between the seizures. For both patients there is a 20 minute post-ictal state with distinct network structures.

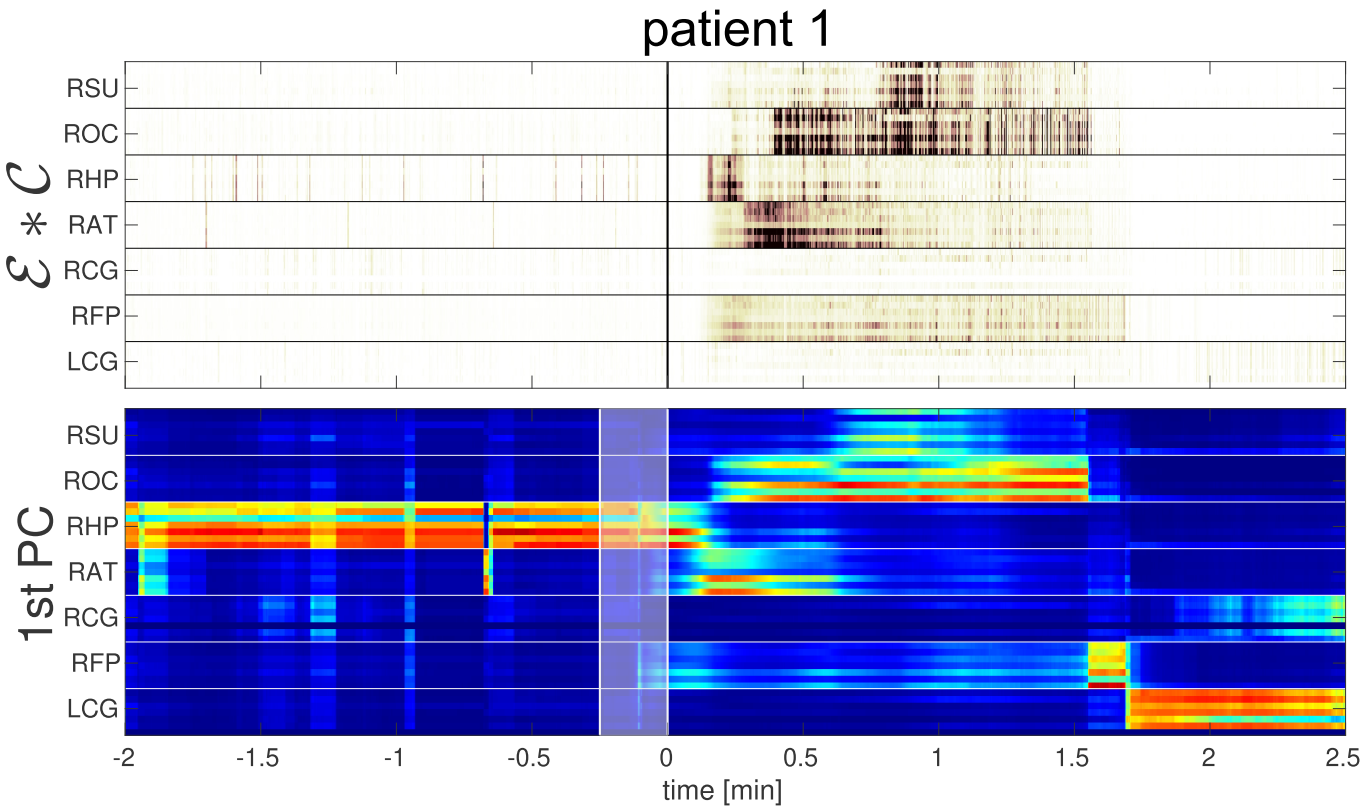

FIG. 11: **Causal sending and first principal components.** Time course for seizure #4 of patient 1 from 2 minutes before seizure onset to 2.5 minutes after. For this patient, we have seven brain regions covered with electrodes. Taking the mean of $\mathcal{C} * \mathcal{E}$ for each brain region leaves us with a 7x7 adjacency matrix for each time window. In the upper plot, these matrices are stratified to show them across time. From this plot, the onset in the right hippocampal region is very distinct. The lower plot shows the first principal components of the upper plots and this highlights the right hippocampal component even before seizure onset.

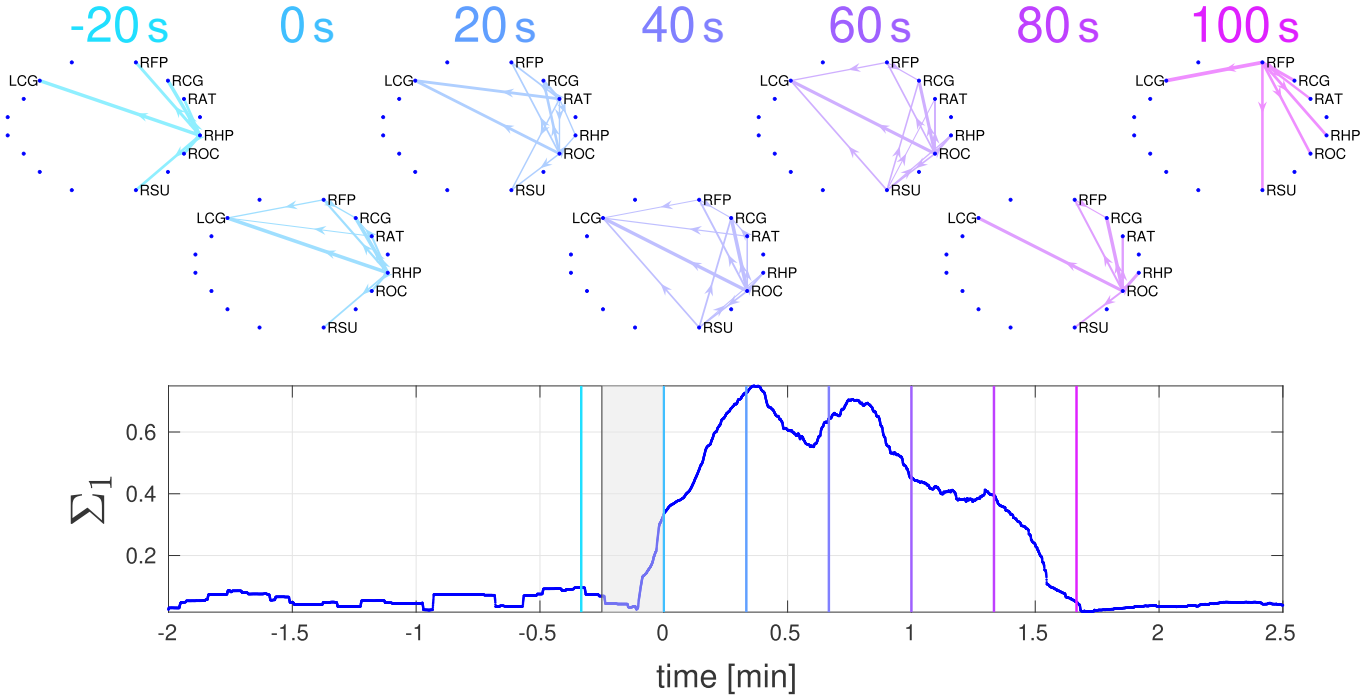

FIG. 12: **Progression of interactions between brain areas before, during and after a seizure.** Network motifs (top panel) around seizure #4 for patient 1. Time 0 indicates seizure onset as determined by the neurologist. The gray box indicates the window length for PCA. The seven lines (cyan to magenta) indicate the times between -20 seconds to 100 seconds in steps of 20 seconds before and after seizure onset. The lower panel shows the first singular value Σ_1.

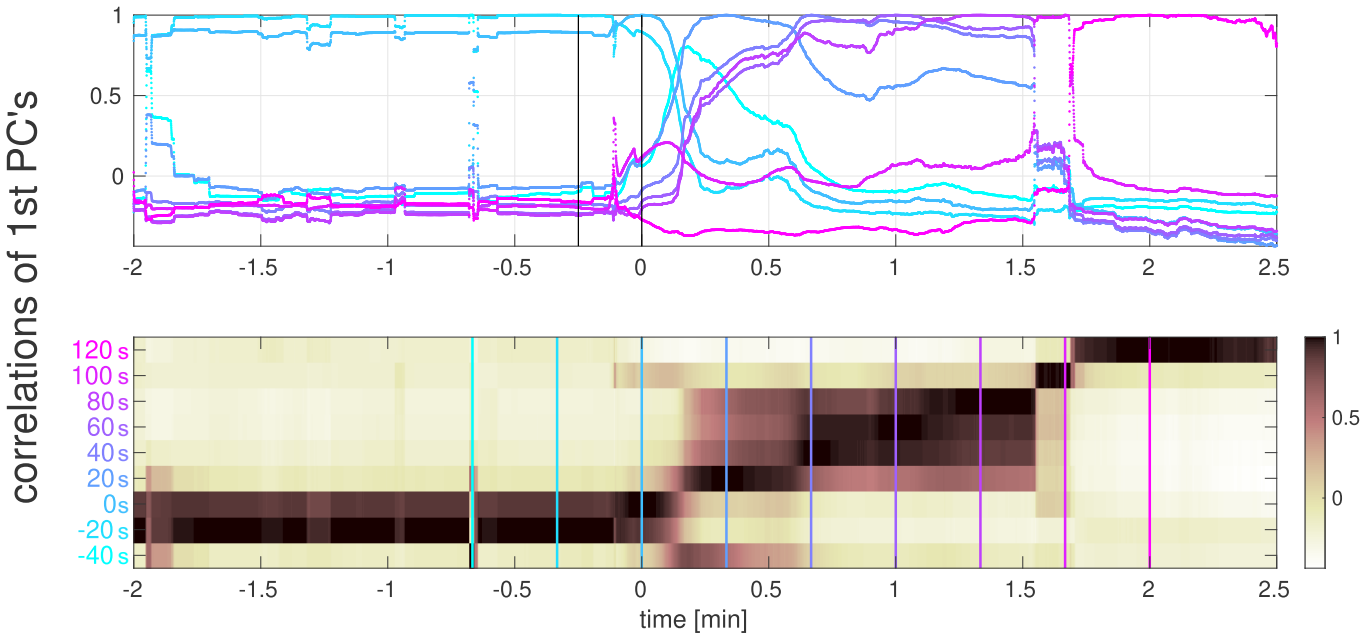

FIG. 13: **Correlations between the first PCs of network motifs.** The top plot shows the correlations of the first PC between -20 seconds and 100 seconds around seizure onset to all the other first PCs over time. The seven colors correspond to the times and colors of Fig. 12. The lower plot shows the heat map of the upper plot. This plot indicates that for each temporal phase around seizures we have distinct network motifs.

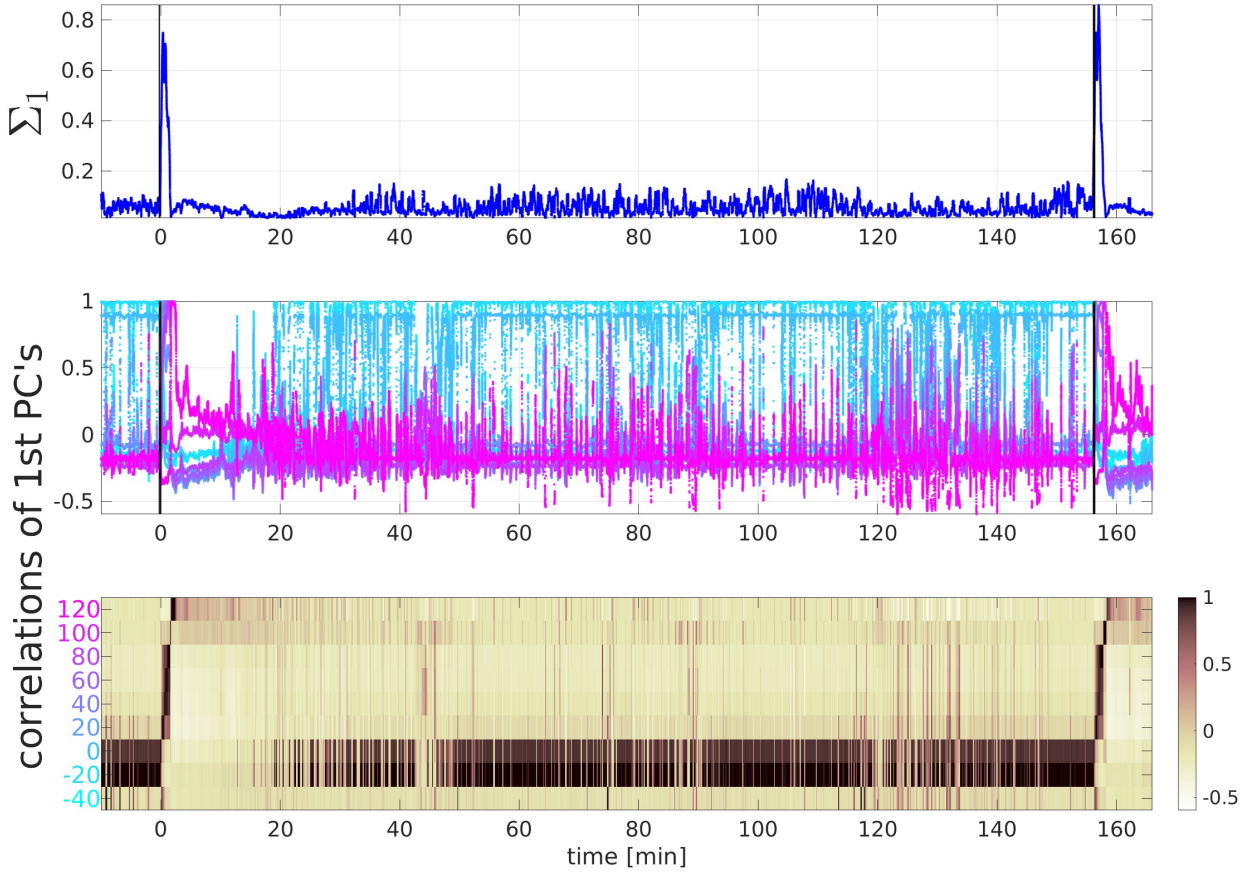

FIG. 14: **Analysis of iEEG recordings for patient 1 starting 10 minutes before seizure #4 to 10 minutes after seizure #5**. Nearly three hours of data are shown. The upper plot shows the first singular value Σ_1 where the two seizures are marked with black lines. The middle and lower plots show the correlations of the first PC between -20 seconds and 100 seconds around seizure onset to all the other first PCs over time. The seven colors correspond to the times and colors of Fig. 12. As seen in the previous figure, each temporal phase around seizures shows distinct network motifs. Interestingly the postictal phase lasts for around 20 minutes.

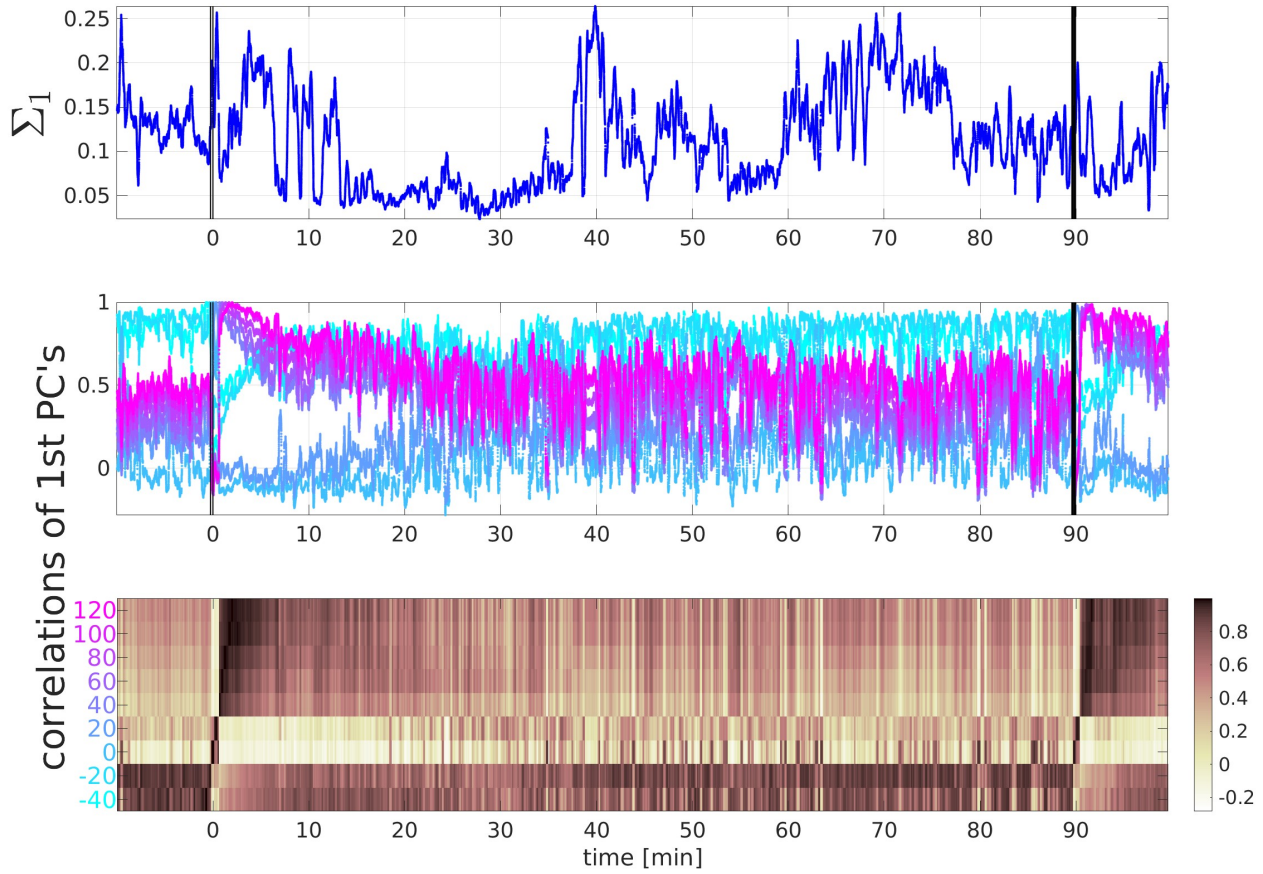

FIG. 15: **Analysis of iEEG recordings for patient 2 starting 10 minutes before seizure #4 to 10 minutes after seizure #5**. These plots are the same as in Fig. 14 for another patient. For this patient about 2 hours of data are shown. As seen in the previous figure, each temporal phase around seizures shows distinct network motifs. The postictal phase for this patient also lasts for around 20 minutes but is less distinct than the previous patient. The two seizures have a smaller first PC during the seizure and higher values between the seizures than the previous patient.

Patient 2 is especially interesting because there are three groups of seizures within the 11 seizures: (i) seizures #1, #2, #9, and #11 stay on the right side of the brain; (ii) seizures #3 and #10 are right progressing to left seizures; and (iii) seizures #4, #5, #6, #7, and #8 occur on the left side of the brain. Three examples of the a_1 values are shown in Fig. 16. The a_1 values for all seizures in each group look very similar.

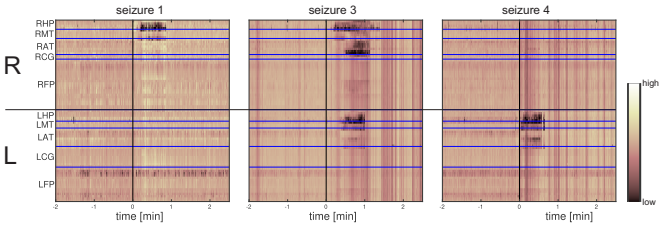

FIG. 16: a_1 value for one example seizure of each group for patient 2: (i) seizures #1, #2, #9, and #11 stay on the right side of the brain; (ii) seizures #3 and #10 are right progressing to left seizures; and (iii) seizures #4, #5, #6, #7, and #8 occur on the left side of the brain. The channels were sorted according to the brain regions used for network analysis.

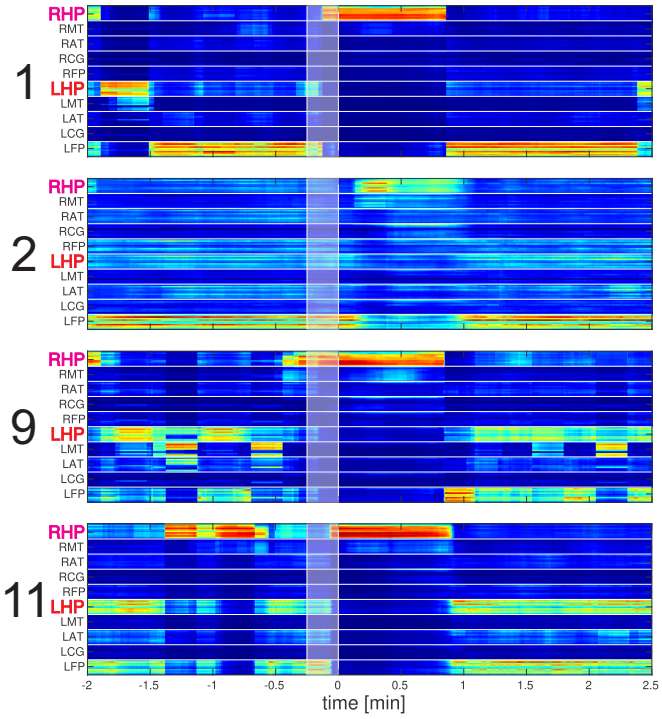

FIG. 17: Correlations between the first PCs of network motifs for patient 2 and seizures #1, #2, #9, and #11. These seizures stay on the right hemisphere. Interestingly, there appear similar preictal network components on the left hemisphere, as for all the other seizures (see Figs. 18 and 19).

In Figs. 17, 18, and 19 we show the correlations of the first PCs for the three seizure groups. While the networks during the seizures are located on the right, both, or left sides

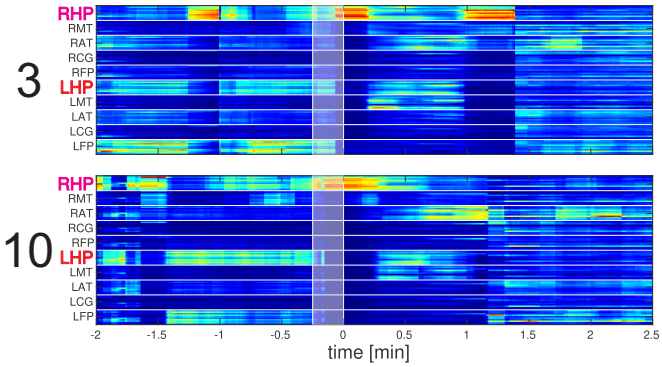

FIG. 18: Correlations between the first PCs of network motifs for patient 2 and seizures #3 and #10. These seizures are progressing from right to left.

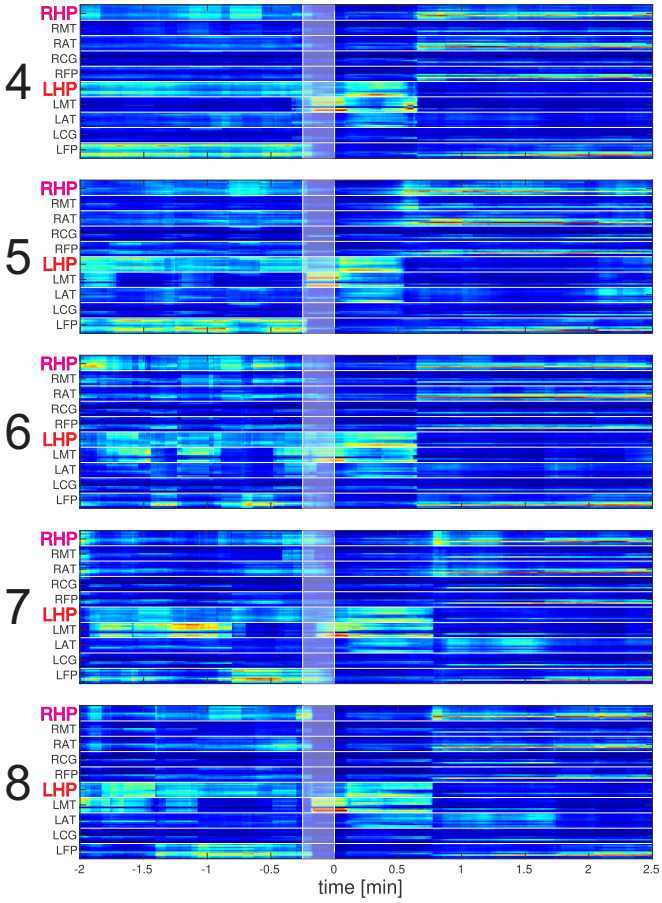

FIG. 19: Correlations between the first PCs of network motifs for patient 2 and seizures #4, #5, #6, #7, and #8 which occur on the left side of the brain.

of the brain, the networks before the seizures are in both hemispheres for all seizures. The seizures originating solely from the right mesial temporal area (RHP; Fig.17) are particularly interesting since this method could identify changes in the dynamics of the left mesial temporal area (LHP), which happens to be another seizure onset region, despite no identifiable iEEG changes on the left side.

It is important to note that there are multiple ways of mapping electrodes to brain regions and subsequently grouping or merging the assigned regions. We classified the regions into eight distinct groups based on proximity, structural similarity, and previous studies. However, larger areas could further be divided into smaller clusters (subnetworks), depending on the specific study. Interestingly, this work showed that even a coarse and heterogeneous grouping of large brain regions is still able to reveal the underlying dynamics that were otherwise not visible. Further work that aims to classify or even forecast seizures might require grouping regions in a different manner.

V. DISCUSSION

We introduced a novel method for extracting network dynamics from data by combining existing flavors of DDA and incorporating PCA into NM-DDA, an analytical framework for identifying network motifs in time series data. To assess the effectiveness of this approach, the method was initially tested on coupled Rössler systems, where the ground truth is known and the dynamics and network structure can be manipulated. Furthermore, the robustness of the method was evaluated by examining its performance under the influence of added white noise. This rather challenging test case, which involved connections between low-dimensional and highly similar nodes, served to validate the effectiveness of the technique.

We also applied NM-DDA to recordings from human brains during epileptic seizures and identified the contributions of different brain regions over the course of a seizure. We probed the underlying dynamical system from intracranial recordings of seizures from two patients: patient 1, whose seizures were determined to be identical based on their electrographic patterns, and patient 2, whose seizures were classified into three different electrographic types, based on their regions of initiation and propagation.

NM-DDA was able to identify the high degree of similarity within each seizure type identified in both patients. Further, the three seizure types in patient 2 could be differentiated based on the changes in dynamics captured by the framework. Intriguingly, we also identified unexpected changes in some regions based on the iEEG recordings. The dynamics in these "hidden" areas may help differentiate seizure types and uncover underlying causes that could not otherwise be detected visually.

These new analytical techniques have the potential to enhance clinical practice in epilepsy diagnostics. For example, our proposed framework could be used to evaluate noninvasive data from patients with epilepsy. Before being implanted with iEEG electrodes, patients receive scalp EEG contacts whose recordings are used to inform the placement of future invasive electrodes. A limited time window is available for capturing these data, and some seizure types from these patients may be missed, resulting in possibly incomplete coverage during iEEG evaluation. The framework we propose may be able to better infer seizure lateralization and might capture other potential regions of interest, which should lead to improved surgical and clinical outcomes.

Another application is to use the dynamics of seizures from different patients to develop a novel seizure classification system. We found that the recordings from dozens of electrodes can be characterized by their average, and that the average retains the dynamics of the recorded regions, allowing for a more efficient comparison of seizure activity across patients. This would provide us with a greater understanding of different seizures and bring us a step closer to providing patient-specific treatments for controlling an individual's epilepsy. DDA is also able to extract relevant dynamics in the presence of noise with minimal preprocessing and can be applied online before and during seizures to provide immediate feedback on their time course.

VI. CONCLUSION

NM-DDA is an analytic framework that could provide useful insights into other complex networks, as evaluated here and in previous studies (see e.g. [23]). Nature abounds with many nonlinear dynamical systems. NM-DDA could be used to identify their networks of nodes and detect subtle changes between them, as we demonstrated in the simulated Rössler example.

Data Availability

The Rössler data used in this work were produced with basic codes for integrating the systems under study by using a Runge-Kutta integration scheme [35]. The iEEG epilepsy data is not currently publicly available as it contains information that could compromise the privacy of the participants. The iEEG data can be made available upon request from the corresponding author.

Acknowledgements

C.L. and T.J.S. were supported by NIH EB026899 and MH132664. P.S. was supported by CDMRP W81XWH-22-1-0315. S.S.C. was supported by NINDS R01-2NS062092. E.M.A.M.M. was supported by CNPq (Grants No. 310788/2021-8 and 405419/2021-0) and FAPEMIG (Grant No. APQ-03197-18).

[1] Amaral, L. A. N. and Ottino, J. M. (2004). Complex networks. *The European Physical Journal B - Condensed Matter*, 38(2):147–162.

[2] Bartolomei, F., Lagarde, S., Wendling, F., McGonigal, A., Jirsa, V., Guye, M., and Bénar, C. (2017). Defining epileptogenic networks: Contribution of SEEG and signal analysis. *Epilepsia*, 58(7):1131–1147.

[3] Bragin, A., Wilson, C. L., and Engel, J. (2000). Chronic epileptogenesis requires development of a network of pathologically interconnected neuron clusters: a hypothesis. *Epilepsia*, 41 Suppl 6(8):S144–S152.

[4] Carvalho, V. R., Moraes, M. F. D., Cash, S. S., and Mendes, E. M. A. M. (2021). Active probing to highlight approaching transitions to ictal states in coupled neural mass models. *PLOS Computational Biology*, 17(1):e1008377.

[5] Dalic, L. and Cook, M. (2016). Managing drug-resistant epilepsy: challenges and solutions. *Neuropsychiatric Disease and Treatment*, Volume 12:2605–2616.

[6] Das, A., Sexton, D., Lainscsek, C., Cash, S. S., and Sejnowski, T. J. (2019). Characterizing brain connectivity from human electrocorticography recordings with unobserved inputs during epileptic seizures. *Neural Computation*, 31(7):1271–1326. PMID: 31113298.

[7] Felsenstein, O., Peled, N., Hahn, E., Rockhill, A. P., Folsom, L., Gholipour, T., Macadams, K., Rozengard, N., Paulk, A. C., Dougherty, D., Cash, S. S., Widge, A. S., Hämäläinen, M., and Stufflebeam, S. (2019). Multi-modal neuroimaging analysis and visualization tool (mmvt). *arXiv*, 1(617):1–29.

[8] Freestone, D. R., Karoly, P. J., Peterson, A. D., Kuhlmann, L., Lai, A., Goodarzy, F., and Cook, M. J. (2015). Seizure Prediction: Science Fiction or Soon to Become Reality? *Current Neurology and Neuroscience Reports*, 15(11).

[9] Hahamy, A., Behrmann, M., and Malach, R. (2015). The idiosyncratic brain: Distortion of spontaneous connectivity patterns in autism spectrum disorder. *Nature Neuroscience*, 18(2):302–309.

[10] Hammond, C., Bergman, H., and Brown, P. (2007). Pathological synchronization in Parkinson's disease: networks, models and treatments. *Trends in Neurosciences*, 30(7):357–364.

[11] Iasemidis, L. D. (2003). Epileptic seizure prediction and control. *IEEE transactions on bio-medical engineering*, 50(5):549–58.

[12] Jirsa, V., Proix, T., Perdikis, D., Woodman, M., Wang, H., Gonzalez-Martinez, J., Bernard, C., Bénar, C., Guye, M., Chauvel, P., and Bartolomei, F. (2017). The Virtual Epileptic Patient: Individualized whole-brain models of epilepsy spread. *NeuroImage*, 145:377–388.

[13] Kramer, M. A. and Cash, S. S. (2012). Epilepsy as a Disorder of Cortical Network Organization. *The Neuroscientist*, 18(4):360–372.

[14] Kremliovsky, M. and Kadtke, J. (1997). Using delay differential equations as dynamical classifiers. *AIP Conference Proceedings*, 411:57.

[15] Kuhlmann, L., Grayden, D. B., Wendling, F., and Schiff, S. J. (2015). Role of multiple-scale modeling of epilepsy in seizure forecasting. *Journal of Clinical Neurophysiology*, 32(3):220–226.

[16] Lainscsek, C., Cash, S. S., Sejnowski, T. J., and Kurths, J. (2021). Dynamical ergodicity DDA reveals causal structure in time series. *Chaos: An Interdisciplinary Journal of Nonlinear Science*, 31(10):103108.

[17] Lainscsek, C., Gonzalez, C. E., Sampson, A. L., Cash, S. S., and Sejnowski, T. J. (2019a). Causality detection in cortical seizure dynamics using cross-dynamical delay differential analysis. *Chaos: An Interdisciplinary Journal of Nonlinear Science*, 29(10):101103.

[18] Lainscsek, C., Rungratsameetaweemana, N., Cash, S. S., and Sejnowski, T. J. (2019b). Cortical chimera states predict epileptic seizures. *Chaos: An Interdisciplinary Journal of Nonlinear Science*, 29(12):121106.

[19] Lainscsek, C., Sampson, A. L., Kim, R., Thomas, M. L., Man, K., Lainscsek, X., The COGS Investigators, Swerdlow, N. R., Braff, D. L., Sejnowski, T. J., and Light, G. A. (2019c). Nonlinear dynamics underlying sensory processing dysfunction in schizophrenia. *Proceedings of the National Academy of Sciences*, 116(9):3847–3852.

[20] Lainscsek, C., Sampson, A. L., Kim, R., Thomas, M. L., Man, K., Lainscsek, X., The COGS Investigators, Swerdlow, N. R., Braff, D. L., Sejnowski, T. J., and Light, G. A. (2019d). Nonlinear dynamics underlying sensory processing dysfunction in schizophrenia. *Proceedings of the National Academy of Sciences*, 116(9):3847–3852.

[21] Lainscsek, C. and Sejnowski, T. (2015). Delay differential analysis of time series. *Neural Computation*, 27(3):594–614.

[22] Lainscsek, C., Weyhenmeyer, J., Cash, S. S., and Sejnowski, T. J. (2017). Delay differential analysis of seizures in multichannel electrocorticography data. *Neural computation*, 29(12):3181–3218.

[23] Lainscsek, C., Weyhenmeyer, J., Hernandez, M., Poizner, H., and Sejnowski, T. (2013). Non-linear dynamical classification of short time series of the Rössler system in high noise regimes. *Frontiers in Neurology*, 4(182).

[24] Li, A., Chennuri, B., Subramanian, S., Yaffe, R., Gliske, S., Stacey, W., Norton, R., Jordan, A., Zaghloul, K. A., Inati, S. K., Agrawal, S., Haagensen, J. J., Hopp, J., Atallah, C., Johnson, E., Crone, N., Anderson, W. S., Fitzgerald, Z., Bulacio, J., Gale, J. T., Sarma, S. V., and Gonzalez-Martinez, J. (2018). Using network analysis to localize the epileptogenic zone from invasive EEG recordings in intractable focal epilepsy. *Network Neuroscience*, 2(2):218–240.

[25] Lorenz, E. N. (1963). Deterministic nonperiodic flow. *J. Atmos. Sci.*, 20:130 – 141.

[26] Maran, M., Grent-'t Jong, T., and Uhlhaas, P. J. (2016). Electrophysiological insights into connectivity anomalies in schizophrenia: a systematic review. *Neuropsychiatric Electrophysiology*, 2(1):6.

[27] Miletics, E. and Molnárka, G. (2004). Taylor series method with numerical derivatives for initial value problems. *J. Comp. Methods in Sci. and Eng.*, 4(1,2):105–114.

[28] Miletics, E. and Molnárka, G. (2005). Implicit extension of Taylor series method with numerical derivatives for initial value problems. *Comput. Math. Appl.*, 50(7):1167–1177.

[29] Mina, F., Benquet, P., Pasnicu, A., Biraben, A., and Wendling, F. (2013). Modulation of epileptic activity by deep brain stimulation: A model-based study of

frequency-dependent effects. *Frontiers in Computational Neuroscience*, 7(JUN):1–16.

[30] Moraes, M. F. D., de Castro Medeiros, D., Mourao, F. A. G., Cancado, S. A. V., and Cota, V. R. (2021). Epilepsy as a dynamical system, a most needed paradigm shift in epileptology. *Epilepsy & Behavior*, 121:106838. NEWroscience 2018.

[31] Mormann, F., Andrzejak, R. G., Elger, C. E., and Lehnertz, K. (2007). Seizure prediction: the long and winding road. *Brain*, 130(2):314–333.

[32] Packard, N. H., Crutchfield, J. P., Farmer, J. D., and Shaw, R. S. (1980). Geometry from a time series. *Phys. Rev. Lett.*, 45:712.

[33] Palus, M. and Vejmelka, M. (2007). Directionality of coupling from bivariate time series: How to avoid false causalities and missed connections. *Phys. Rev. E*, 75.

[34] Planck, M. (1900). Über irreversible Strahlungsvorgänge. *Annalen der Physik*, 306(1):69–122.

[35] Press, W., Flannery, B., Teukolsky, S., and Vetterling, W. (1990). *Numerical Recipes in C*. Cambridge University Press, New York, NY, USA.

[36] Richardson, M. P. (2012). Large scale brain models of epilepsy: Dynamics meets connectomics. *Journal of Neurology, Neurosurgery and Psychiatry*, 83(12):1238–1248.

[37] Rössler, O. E. (1976). An equation for continous chaos. *Physics Letters A*, 57:397.

[38] Salami, P., Peled, N., Nadalin, J. K., Martinet, L. E., Kramer, M. A., Lee, J. W., and Cash, S. S. (2020). Seizure onset location shapes dynamics of initiation. *Clinical Neurophysiology*, 131(8):1782–1797.

[39] Sampson, A. L., Lainscsek, C., Gonzalez, C. E., Ulbert, I., Devinsky, O., Fabó, D., Madsen, J. R., Halgren, E., Cash, S. S., and Sejnowski, T. J. (2019). Delay differential analysis for dynamical sleep spindle detection. *Journal of Neuroscience Methods*, 316:12–21. Methods and models in sleep research: A Tribute to Vincenzo Crunelli.

[40] Sauer, T., Yorke, J. A., and Casdagli, M. (1991). Embedology. *Journal of Statistical Physics*, 65:579.

[41] Soper, D. J., Reich, D., Ross, A., Salami, P., Cash, S. S., Basu, I., Peled, N., and Paulk, A. C. (2023). Modular pipeline for reconstruction and localization of implanted intracranial ECoG and sEEG electrodes. *PLOS ONE*, 18(7):e0287921.

[42] Stacey, W., Kramer, M., Gunnarsdottir, K., Gonzalez-Martinez, J., Zaghloul, K., Inati, S., Sarma, S., Stiso, J., Khambhati, A. N., Bassett, D. S., Smith, R. J., Liu, V. B., Lopour, B. A., and Staba, R. (2020). Emerging roles of network analysis for epilepsy. *Epilepsy Research*, 159(October 2019):106255.

[43] Stam, C. J., Jones, B. F., Nolte, G., Breakspear, M., and Scheltens, P. (2007). Small-world networks and functional connectivity in Alzheimer's disease. *Cerebral Cortex*, 17(1):92–99.

[44] Stanley, H. E. (1999). Scaling, universality, and renormalization: Three pillars of modern critical phenomena. *Reviews of Modern Physics*, 71(2):S358–S366.

[45] Takens, F. (1981). Detecting strange attractors in turbulence. In Rand, D. A. and Young, L.-S., editors, *Dynamical Systems and Turbulence, Warwick 1980*, volume 898 of *Lecture Notes in Mathematics*, pages 366–381. Springer Berlin/Heidelberg.

[46] Tononi, G., Sporns, O., and Edelman, G. M. (1994). A measure for brain complexity: Relating functional segregation and integration in the nervous system. *Proceedings of the National Academy of Sciences of the United States of America*, 91(11):5033–5037.

[47] Uhlhaas, P. J. and Singer, W. (2006). Neural Synchrony in Brain Disorders: Relevance for Cognitive Dysfunctions and Pathophysiology. *Neuron*, 52(1):155–168.

[48] Van Diessen, E., Diederen, S. J. H., Braun, K. P. J., Jansen, F. E., and Stam, C. J. (2013). Functional and structural brain networks in epilepsy: What have we learned? *Epilepsia*, 54(11):1855–1865.

[49] Watts, D. J. and Strogatz, S. H. (1998). Collective dynamics of 'small-world' networks. *Nature*, 393(6684):440–442.

[50] Yaffe, R. B., Borger, P., Megevand, P., Groppe, D. M., Kramer, M. A., Chu, C. J., Santaniello, S., Meisel, C., Mehta, A. D., and Sarma, S. V. (2015). Physiology of functional and effective networks in epilepsy.

[51] Yang, J. C., Paulk, A. C., Salami, P., Lee, S. H., Ganji, M., Soper, D. J., Cleary, D., Simon, M., Maus, D., Lee, J. W., Nahed, B. V., Jones, P. S., Cahill, D. P., Cosgrove, G. R., Chu, C. J., Williams, Z., Halgren, E., Dayeh, S., and Cash, S. S. (2021). Microscale dynamics of electrophysiological markers of epilepsy. *Clinical Neurophysiology*, 132(11):2916–2931.

[52] Zijlmans, M., Zweiphenning, W., and van Klink, N. (2019). Changing concepts in presurgical assessment for epilepsy surgery. *Nature Reviews Neurology*, 15(10):594–606.